Presented at the 2012 MPIF / APMI International Conference on Powder Metallurgy & Particulate Materials held in Nashville, USA in June 2012 and published in the Advances in Powder Metallurgy & - 2012 conference proceedings available from the Metal Powder Industries Federation.

Development and Properties of a New Malleable Iron Powder Grade

F. Chagnon and C. Coscia

Rio Tinto Metal Powders

ABSTRACT

Density plays a key role in improving the performance of PM parts. Currently, increased density can be reached through the use of special compacting processes like warm pressing or warm die compaction, double press double sintering, repressing, surface densification or powder forging. Also, to meet specific application requirements, the use of low alloy steel with addition of copper and nickel are often required to increase the tensile properties.

A novel ferrous powder grade was developed to compete with ductile iron. This new malleable iron powder, MIP, is an iron-graphite composite powder in which the carbon is dispersed as graphite nodules in a ferritic matrix. This material achieves nearly 100% densification through liquid phase sintering at 1160°C to a final density of 7.5 g/cm³. Tensile and yield strengths of 800 and 540 MPa, respectively, with an apparent hardness of 30 HRC are reached with a pearlitic matrix structure.

INTRODUCTION

Increasing final density is the most efficient way to improve the static and dynamic properties of PM parts. Higher green density can be achieved through the use of more efficient lubricants that, when admixed at lower concentrations and/or in combination with the die wall lubrication technique makes possible to reach an increased final density[1,2,3,4,5]. The use of warm compaction or warm die compaction techniques, that lead to larger particle deformation caused by the reduction of the yield strength of steel when the temperature increases, is another means to raise the final density of PM steel parts[5,6,7,8]. However, all these processes currently result in a maximum sintered density of about 7.45 g/cm³ (i.e. 95% relative density) after sintering.

Supersolidus liquid phase sintering (SLPS) is another way to achieve high density. This process requires prealloyed powders that, when heated to an intermediate temperature between the solidus and liquidus, nucleate a liquid within each particle. The amount of liquid produced is a function of the alloy composition and sintering temperature. The individual particles partially melt and hence promote densification by capillary induced rearrangement[9-10]. Indeed, SLPS is possible with the Fe-C system. As shown in Figure 1, when heated above about 1154°C, a Fe-2.1C alloy[11] will start melting and the quantity of the liquid produced will be a function of the carbon concentration and temperature.

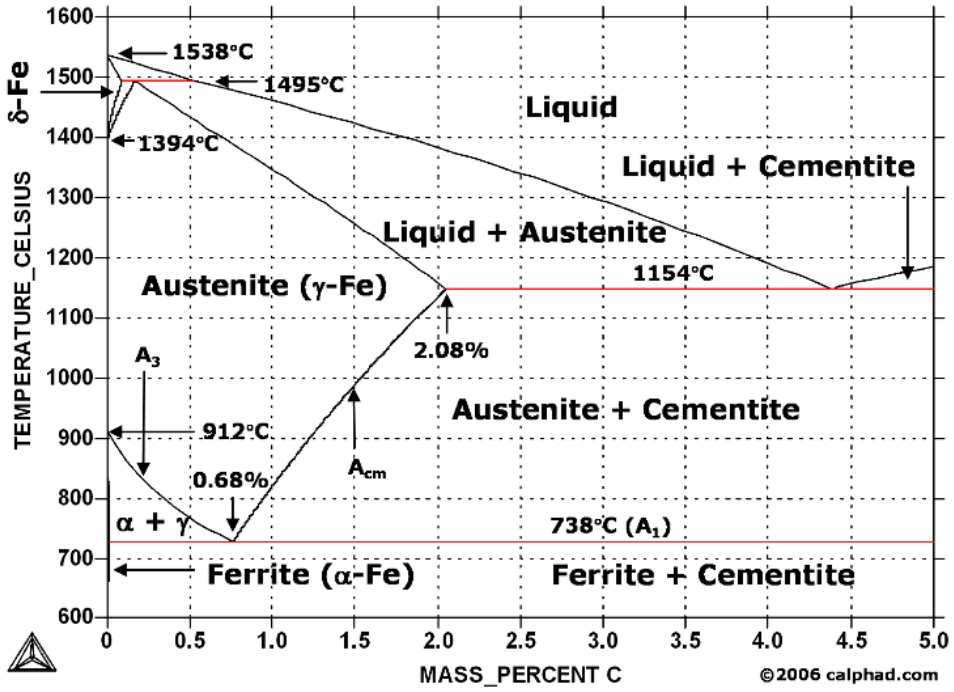

Figure 1. Iron-carbon phase diagram[16].

Some studies were undertaken to develop fully dense parts using this technology. Kimura and al.[12] described a hot pressing process of a Fe-2.0% graphite mixture to reach 7.55 g/cm³ at 1170°C under a pressure of 1 MPa. No mention was made about the resulting microstructure, but the bending strength of 862 MPa suggests that the microstructure was probably carbidic. Shivanath and al.[13] and Young[14] described a process to achieve a density of 7.75 g/cm³ through supersolidus liquid phase sintering of a Fe-0.85Mo-0.4Si-1.35C alloy sintered at 1280°C, where the Si and C are introduced using SiC and graphite. The alloy is fast cooled to room temperature and then submitted to a carbide spheroidization heat treatment to improve the mechanical properties. Khraisat and al.[15] reported that a Fe-1.6C-2Si system produced from admixing FeSi and graphite to an unalloyed iron powder achieves a 95% relative density when sintered between 1250 and 1260°C. Tensile strength values in the order of 350 MPa are reported in the as-sintered condition and 630 MPa for fast cool conditions. Finally, Semel[16] described a method to produce high density ferrous parts by iron infiltration of a high carbon alloy. Both the base iron part and infiltrant are pressed from unalloyed iron powders mixed with free graphite and silicon carbide or ferrosilicon and sinterinfiltrated at 1177°C. A tensile strength of 484 MPa is claimed for a sintered density of 7.47 g/cm³. The tensile strength can be improved by the use of low alloy steel powder or admixing of nickel or copper powders.

One of the main challenges with these materials, is to achieve a microstructure that will allow to reach optimal static and dynamic properties. The objective of this paper is to present the outcome of R&D

work carried out to develop a new Fe-2C-1Si powder that reaches full density through SLPS and achieve a pearlitic-graphitic matrix structure showing a good compromise between mechanical properties and machinability and could hence be used to replace parts currently made of ductile iron (DI), malleable iron or compacted graphite iron (CGI) castings.

EXPERIMENTAL PROCEDURE

Malleable cast iron is produced from white cast iron submitted to a heat treatment named malleabilization[17-18]. During this heat treatment, graphite nucleates from the cementite of the white iron to form nodules. For a successful heat treatment, the presence of silicon is also required to promote graphitization. Furthermore, silicon lowers the solubility of carbon in both the eutectic and eutectoid and therefore causes the eutectic and eutectoid reactions to take place over a range of temperatures and at a higher temperature than in the Fe-C system[17-19]. The malleabilization treatment is generally carried out in two steps, Figure 2. The first step consists of putting carbon in solution in austenite and is followed by a second stage where an annealing treatment is used to precipitate graphite as nodules. The temperature and time to perform this treatment is a function of the chemical composition and the size of the castings.

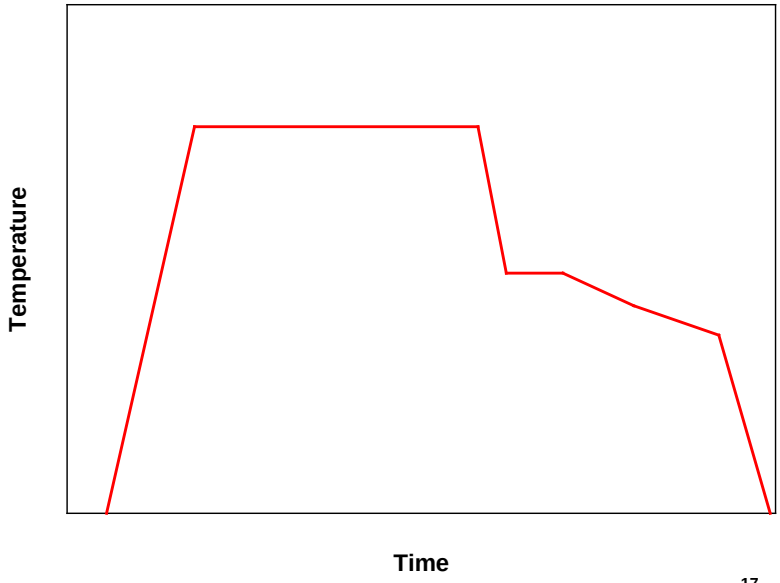

Figure 2. Temperature profile for malleabilizing white cast iron[17].

This concept was applied to the development of a malleable iron powder and is described by Gagné and al.[19]. Indeed, a powder particle can be seen as a small ingot submitted to a malleabilization treatment. Table 1 summarizes the chemical and physical properties of this new malleable iron powder grade, MIP. The carbon and silicon concentrations have been optimized to achieve a fully ferritic structure to maximize powder compressibility and optimize the sinterability. Figure 3 illustrates the typical shape of MIP particles and the distribution of the graphite nodules within the particles. The shape of this new water atomized powder is irregular. During the annealing treatment, graphite nodules are evenly precipitated in the core and at the surface of the particles. The iron matrix is fully ferritic to improve compressibility. Because the graphite is embedded in the iron matrix, no segregation occurs and unlike regular iron-graphite blends, the flow rate is not affected by the presence of free graphite particles.

Table 1. Chemical and physical properties of MIP.

C, %	O, %	Si, %	S, %	+60 mesh, %	-60/+100 mesh, %	-100/+325 Mesh, %	-325 mesh, %	Apparent density, g/cm³	Flow, s/50g
1.97	0.10	1.05	0.001	Trace	17	63	20	2.85	30

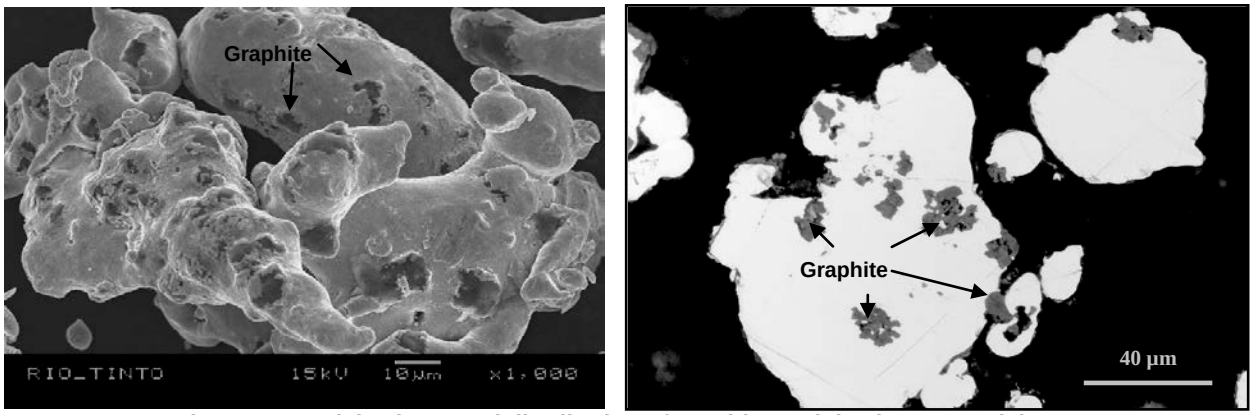

Figure 3. Particle shape and distribution of graphite nodules in MIP particles.

The compressibility and the green strength of this new powder grade was determined with a mix containing 0.5% wax pressed at 415, 550, 620 and 690 MPa. The sintering behaviour was evaluated by dilatometry with 2.54 X 0.64 X 0.64 cm specimens sintered at 1165°C. Rectangular bars (7.6 X 1.3 X 1.2 cm) were also pressed to various green densities to evaluate the effect of sintering temperature and green density on dimensional change and sintered densities. The resulting test bars were machined into tensile, fatigue or unnotched impact energy specimens (MPIF Standards 10, 56 and 40, respectively). The axial fatigue strength was evaluated at a load ratio of R = -1 using the staircase method with a run out limit of 10 millions cycles. Specimens of 3.18 X 1.27 X 0.64 cm were used to measure the transverse rupture strength (MPIF 41).

The sintering behaviour was studied with a dilatometer at 1166°C for 10 minutes under a $90N_2/10H_2$ atmosphere while the effect of the sintering profile was evaluated in a laboratory furnace to accurately control the heating and cooling rates. The properties of specimens sintered at 1152, 1156, 1158, 1162 and 1166°C and a holding time of 10 minutes at temperature were measured. Corresponding sintering temperature profiles consisted of a heating rate of 1°C/min. from 1140 to the sintering temperature, a cooling rate of 1°C/min. to 1140°C in order to avoid the precipitation of eutectic carbides, and a cooling at 30°C/min. from 1140 to 800°C to prevent the precipitation of eutectoid carbides. Cooling during the "$\gamma \rightarrow \alpha$+carbide" phase transformation was maintained at ~1°C/s. Figure 4 shows typical temperature profiles used for the dilatometry and the sintered properties evaluation. The microstructure was observed before and after etching by optical microscopy. The graphite shape was quantified by the image analysis technique.

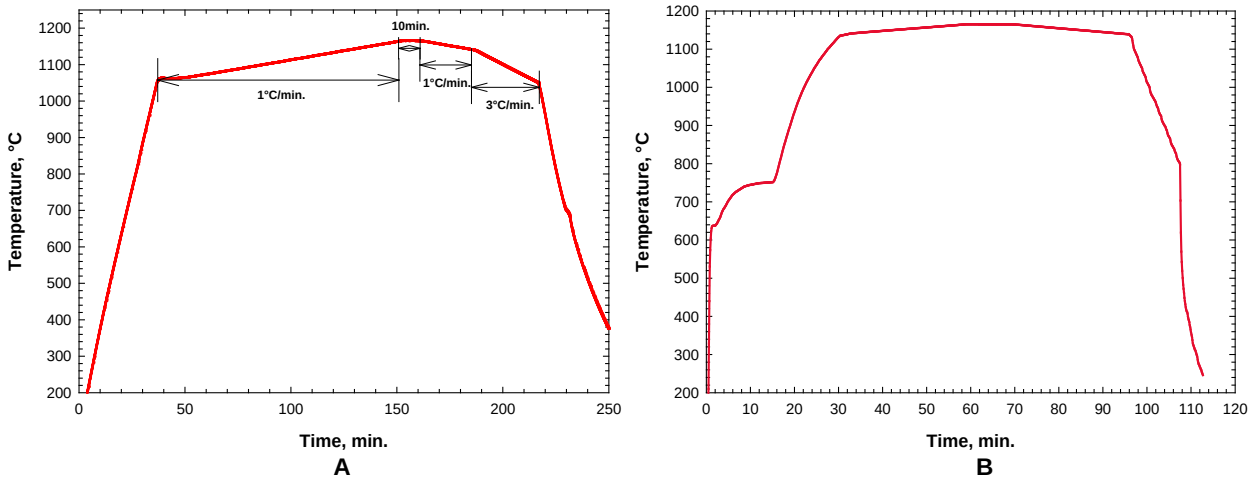

Figure 4. Temperature profiles used for dilatometer study (A) and evaluation of the sintered properties (B).

RESULTS AND DISCUSSION

Green properties

The compressibility curve of MIP is illustrated in Figure 5a. A density of 6.6 g/cm³ can be reached at 560 MPa (40 tsi). Compared to standard water atomized steel powder, this value seems low but it is worth noting that MIP contains about 2% free graphite, which is significantly lower in density than iron. On a relative density basis, at 560 MPa (40 tsi) a value of about 91.7% is achieved comparatively to about 93.5% for a FL-4400 steel powder mixed with 0.5% lubricant[5]. The variation of green strength with the green density of specimens pressed with MIP is shown in Figure 5b. Green strength increases linearly with green density. At 6.6 g/cm³, a value of 9.3 MPa (1350 psi) is reached, which is adequate for the compaction of complex PM parts.

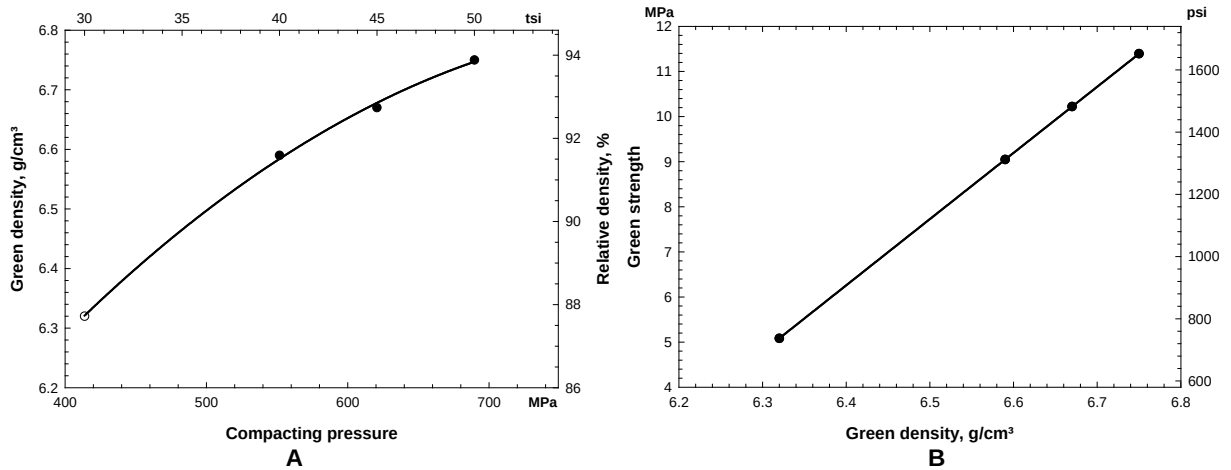

Figure 5. Compressibility of MIP (A) and variation of green strength with density (B) of specimens pressed with MIP (mix with 0.5% wax).

Microstructure and dilatometry behaviour

SLPS of an Fe-2C-Si alloy requires a specific sintering temperature profile to achieve full density without distortion and gas entrapment in the core of the specimens. The former can be realized with proper heating rate and sintering temperature window while for the latter, the iron oxides must be reduced before appearance of the first liquid. Furthermore, given that the liquid cast iron contains a high concentration of carbon, the cooling rate during solidification must be reduced in order to avoid the precipitation of eutectic carbides. Similarly, the cooling rate in the austenite phase must be controlled to minimize the precipitation of eutectoid carbides. Figure 6a illustrates a typical unetched microstructure obtained at optimal sintering conditions, while Figure 6b shows the effect of gas entrapment in the core of a specimen. The latter can be minimized by lowering the heating rate prior to the onset of densification. Figure 7 illustrates a typical microstructure of an over-sintered specimen. High sintering temperature (>1170°C) and/or long sintering time favours the complete dissolution of graphite in either the austenite or the liquid phase. This essentially results in the elimination of graphite nucleation sites for carbon precipitation upon cooling. So, as the material achieves full density and if all the nucleation sites have been dissolved, carbon will precipitate at the grain boundaries or within the liquid phase with a flaky graphite structure. The number of large flakes can impact the static properties but more importantly the dynamic properties which will be discussed in the following sections.

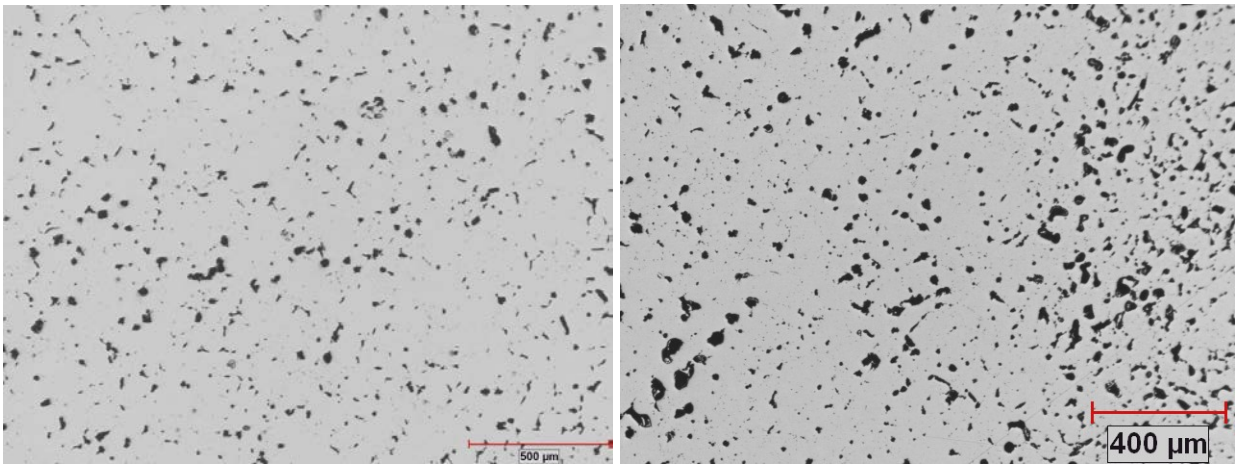

A B

Figure 6. Unetched microstructure of a properly sintered MIP specimen (A); 50X. and of one in which gas entrapment occurred in the core of specimen (B)

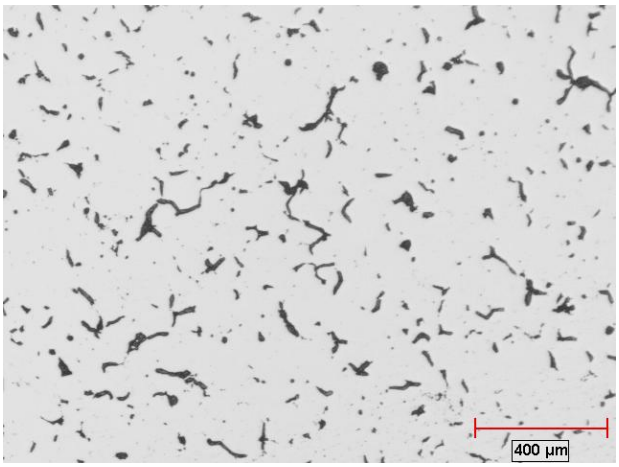

Figure 7. Typical unetched microstructure of an over sintered MIP specimen.

Figure 8 shows typical etched microstructures of specimens processed with cooling rates of 5 and 1°C/min., respectively, in the 1166 to 1140°C range. Both specimens exhibit an almost fully pearlitic structure with graphite particles. Some ferrite is present around the graphite particles at a cooling rate of 1°C/min. while a few carbides appear at the grain boundaries when the cooling rate is increased to 5°C/min.

Figure 9 illustrates the variation of dimensional change of a MIP specimen pressed at 6.6 g/cm^3. The heating rate from 1080 to 1165°C was 1°C/min. with a time at temperature of 10 minutes, a cooling rate of 1°C/min. from 1166 to 1140°C and 3°C/min. from 1140 to 1050°C. Upon heating to 760°C, the specimen expands at a rate of about 0.0016%/°C, corresponding to the coefficient of thermal expansion in the α phase. The phase transformation α–γ occurs in the range of 760 to 840°C. No significant dimensional change takes place during the phase transformation, as graphite diffusion occurs very quickly because the nodules are already embedded in the iron matrix unlike admixed graphite in steel powder mixes. However, because of the high carbon concentration, expansion due to carbon diffusion is significant. Indeed, within 840 to 1060°C, the growth related to thermal expansion in the γ phase is 0.0020%/°C while that related to carbon diffusion is about 0.0031%/°C. As the temperature reaches 1060°C, expansion is overcame by the shrinkage. The rate of shrinkage from 1060 to 1100°C is approximately 0.0057%/°C and raises to up 0.010%/°C in the range of 1100 to 1140°C. At 1140°C the rate of shrinkage increases significantly, reaching its highest value from 1156°C, when the first liquid appears, to 1165°C with a rate of 0.27%/°C. The specimen contracts by about 2.5% in this temperature range. It is for this reason that the heating rate must be reduced from 1140°C, to minimize gas entrapment in the core of the specimen. At 1165°C, the specimen shrinks by about 0.8% or 0.08%/minute and the shrinkage stops after 10 minutes as the specimen reaches its full density.

On cooling, contraction is explained by the coefficients of thermal expansion in the γ phase (i.e. 0.0020%/°C) and in α+carbide phase (0.0014%/°C). The phase transformation $\gamma \rightarrow \alpha$+carbide starts at about 700°C and ends at 680°C. The complete sintering cycle results in a contraction of almost 4.0% from green size.

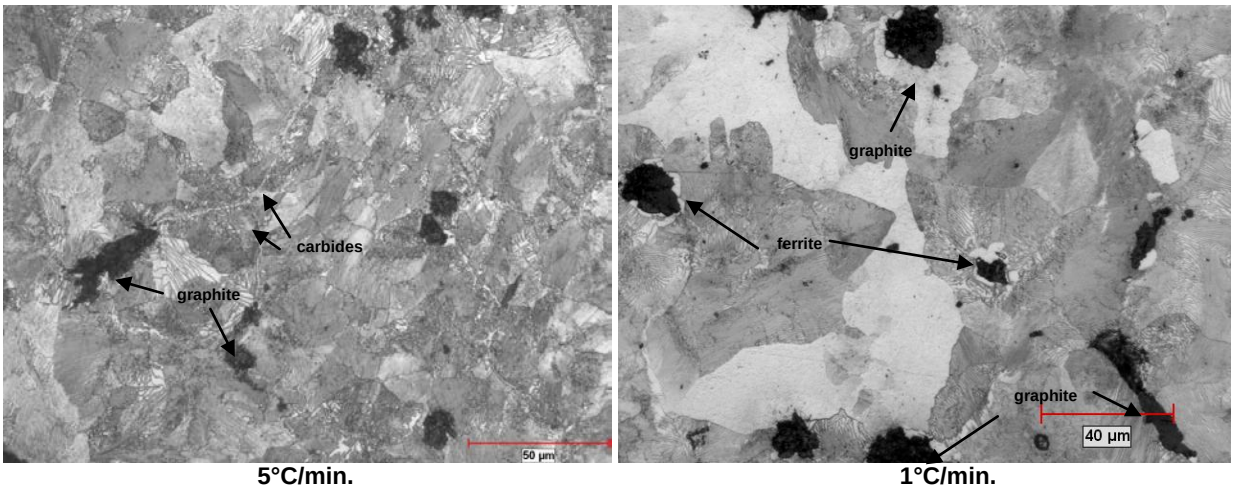

5°C/min. 1°C/min.

Figure 8. Effect of cooling rate from 1166 to 1140°C on microstructure of sintered specimens made with MIP (Nital etching; 500X).

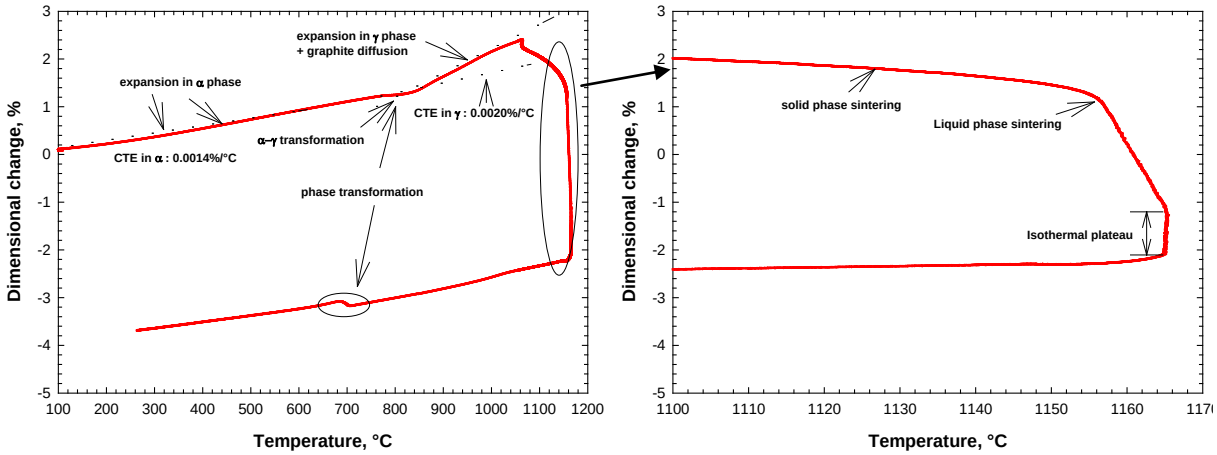

Figure 9. Dimensional change variation of MIP material as a function of temperature (green density of 6.6 g/cm³).

Effect of temperature on sintered properties

Tests were carried out to determine the sintering temperature window of bars pressed with this new powder and to characterize the resulting sintered properties. TRS specimens and rectangular bars were pressed at 45 tsi (i.e. 6.67 g/cm³) and sintered in a laboratory furnace, with a 90% nitrogen/10% hydrogen atmosphere, at 1152, 1156, 1158, 1162 and 1166°C. The following conditions were also maintained during the sintering of the test specimens: a heating rate of 1°C/min. from 1140°C to the sintering temperature, a holding time of 10 minutes at temperature, a cooling rate of 1°C/min. to 1140°C to avoid eutectic carbide precipitation, and 30°C/min. from 1140 to 800°C to avoid eutectoid carbide formation. Sintered specimen characterisation results are summarized in Table 2.

Figure 10 illustrates the correlation between final density and sintering temperature. The bars shrink from -2.94% at 1152°C to about -3.6% at 1158°C. In the range of 1158 to 1166°C, the degree of shrinkage is fairly consistent at -3.57 to -3.66% and the bars reach relative densities of 99.4-99.7% (7.55-7.58 g/cm³). The unetched microstructure of specimens sintered at 1152 to 1166°C is shown in Figure 11. At 1152°C,

about 3% residual porosity remains in the specimen. While some graphite is present in the form of small nodular clusters, most of it has precipitated in the residual pores.

Table 2. Sintered properties of specimens pressed with MIP.

Sintering temperature, °C	1152	1156	1158	1162	1166
Dimensional change, % vs die size	-2.94	-3.39	-3.63	-3.66	-3.57
Density, g/cm³	7.38	7.52	7.55	7.57	7.58
Relative density, %	97.1	99.0	99.4	99.6	99.7
Tensile strength, MPa (ksi)	765 (111)	767 (111)	788 (114)	787 (114)	771 (112)
Yield strength, MPa (ksi)	516 (75)	540 (78)	493 (71)	522 (76)	542 (79)
Elongation, %	2.12	1.80	2.84	2.18	1.84
Transverse rupture, MPa (ksi)	1503 (218)	1763 (256)	1688 (245)	1683 (244)	1767 (256)
Hardness, HRC	25	28	28	29	31

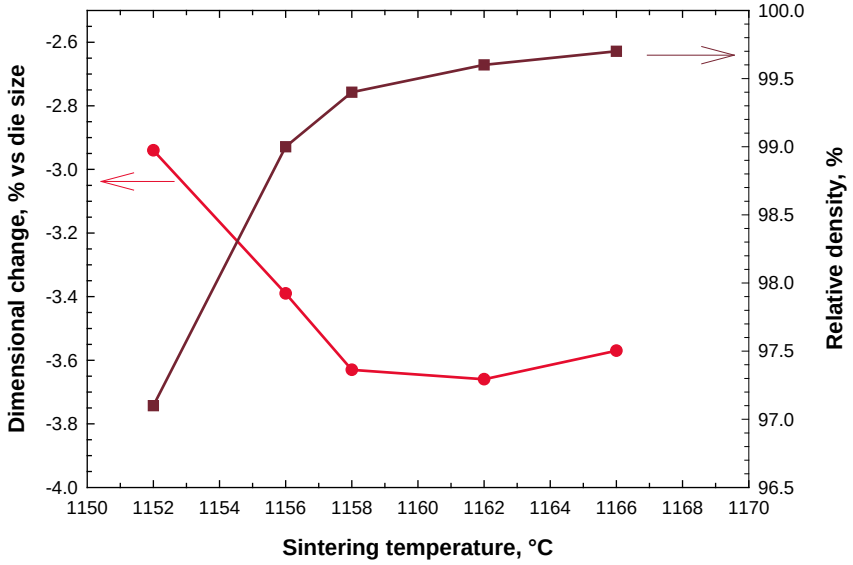

Figure 10. Effect of sintering temperature on dimensional change and relative density.

At 1156°C, only 1% residual porosity is present in the specimen and small graphite flakes can be seen in the microstructure. The latter can be explained by the reduction of residual porosity which was acting as preferential sites for graphite precipitation. Indeed, the volume of liquid having a high carbon concentration increases with sintering temperature. On cooling, carbon will precipitate either as a carbide or in the form of free graphite depending on the cooling rate. With less residual porosity, on cooling, the graphite is more likely to precipitate at the γ grain boundaries and as flakes within the liquid phase, explaining the change in the graphite shape. This being said, a further increase of the sintering temperature will result in a larger fraction of carbon rich liquid phase; hence, resulting in less nodularity and an increase of the size of the graphite flakes. This is clearly illustrated in Figure 12. Indeed, the nodularity decreases from about 70% at 1152°C to about 50% at 1166°C, while the mean length of the flaky graphite particles increases from 28 to 32 µm. It is also worth noting that the number of flakes with a length larger than 100 µm increases from 0.2/mm² at 1152°C to about 1.2/mm² for the specimens sintered at 1158 to 1166°C. Finally, within this temperature range, the number of cluster/mm² lies between 350 to 550. Based on the carbon concentration in the sintered specimens, the carbon content of the austenite and the eutectic, the proportion of liquid phase between 1158 and 1166°C is estimated to be within 4.6 to 7%. Below 4.6%, the structure is under sintered while above 7% liquid, there is a risk of

over sintering and achieving a microstructure similar to that shown in Figure 7. Figure 13 illustrates typical etched microstructures of specimens sintered at 1162°C. These exhibit a fine pearlitic structure with graphite particles showing some ferrite at their periphery.

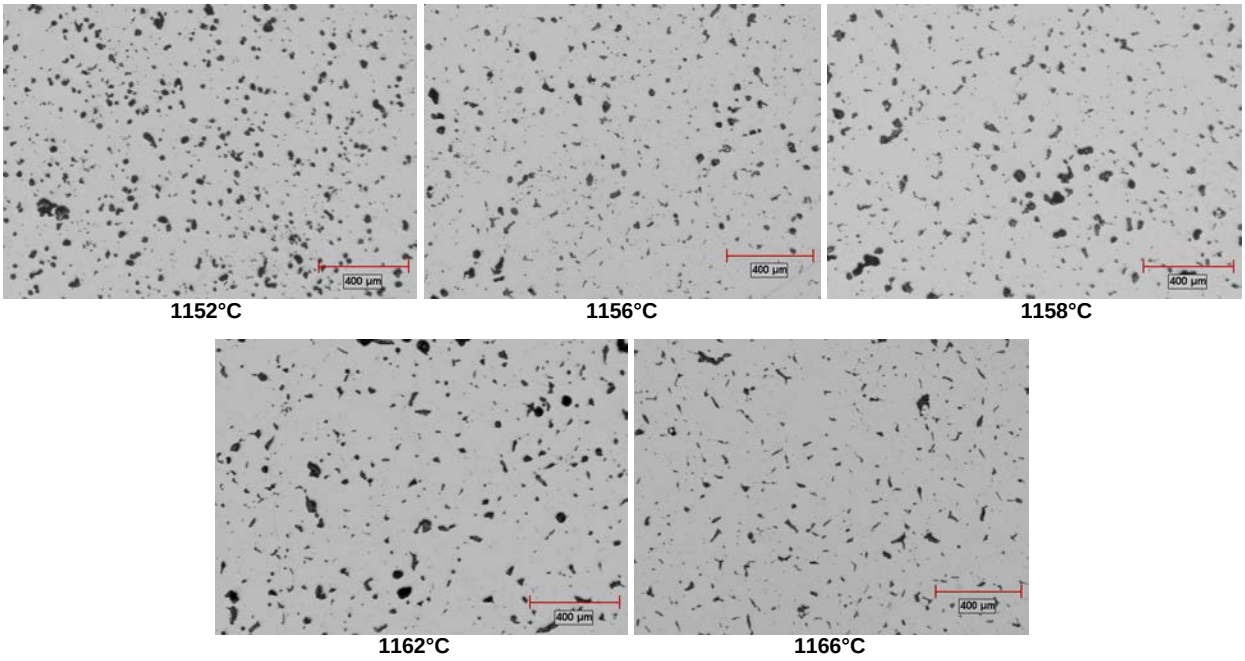

Figure 11. Unetched microstructure of rectangular bars sintered in the range of 1152 to 1166°C (50X).

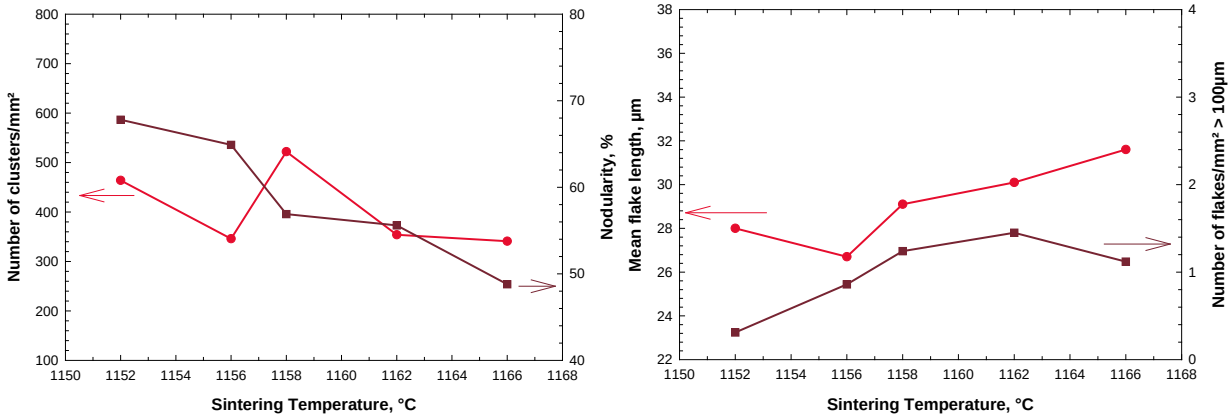

Figure 12. Variation of the number of clusters/mm², nodularity, mean flake length and number of flakes/mm² > 100 µm as a function of sintering temperature of specimens made with MIP.

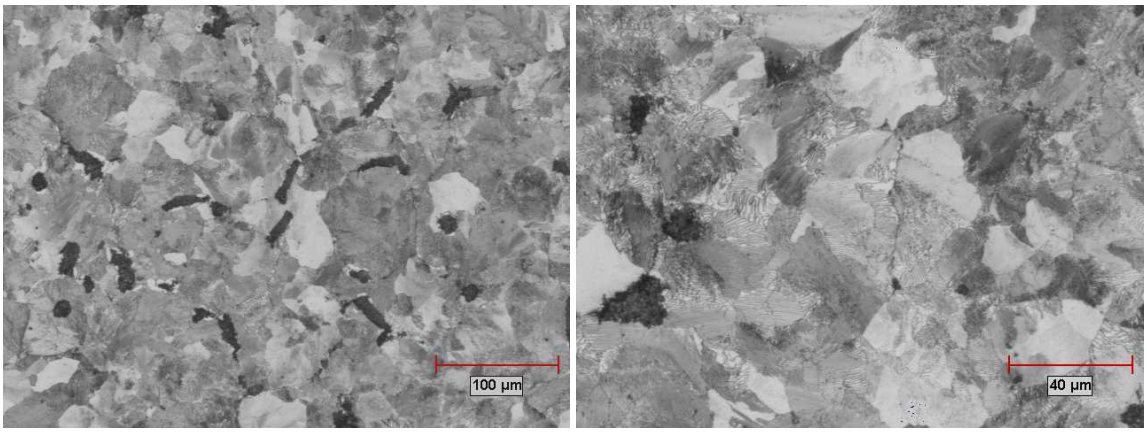

Figure 13. Microstructure of MIP specimens sintered at 1162°C, after Nital etching.

The evolution of the tensile properties with sintering temperature is shown in Figure 14. It is interesting to note that the sintering temperature does not have a significant effect on tensile properties with an average tensile strength of 776±11 MPa (113±2 ksi), an average yield strength of 523±20 MPa (76±3 ksi) and an average elongation of 2.2±0.4% when the sintering temperature increases from 1152 to 1166°C. These values are comparable to that of pearlitic malleable cast iron class 80002 and ductile iron grade 100-70-03[17]. It is worth noting that the tensile properties of MIP materials remain quite consistent even with a significant variation in sintered density (i.e. from 7.38 to 7.58 g/cm³) and the shape of the graphite particles.

Figure 15 illustrates the evolution of transverse rupture strength (TRS) and hardness in the sintering temperature range of 1152 to 1166°C. TRS increases from 1500 MPa (217 ksi) at 1152°C to about 1725 MPa (250 ksi) from 1156 to 1166°C. Hardness increases linearly from 25 HRC at 1152°C to 31 HRC at 1166°C. The latter can be explained by the increase of the sintered density.

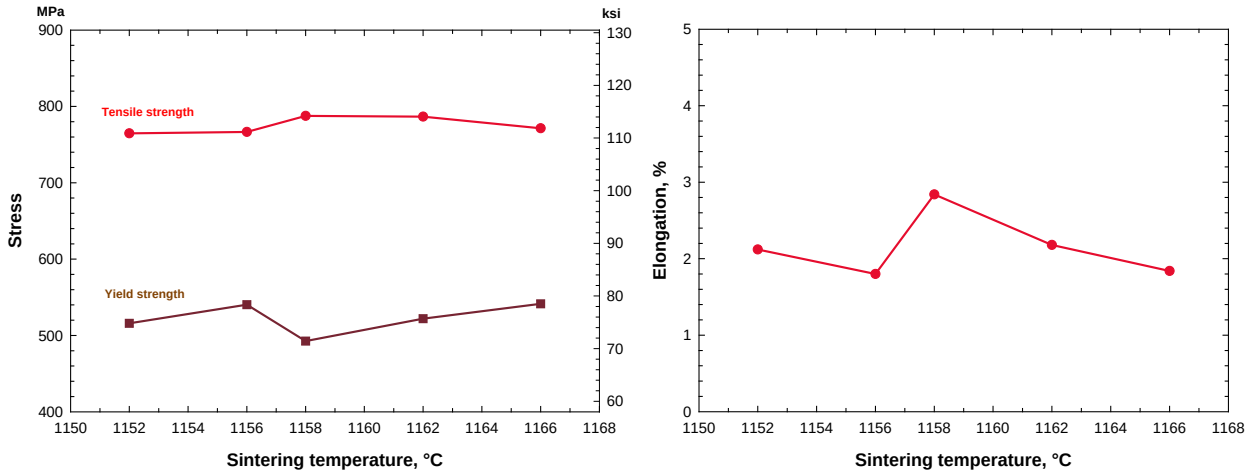

Figure 14. Evolution of the tensile properties with sintering temperature of specimens made with MIP.

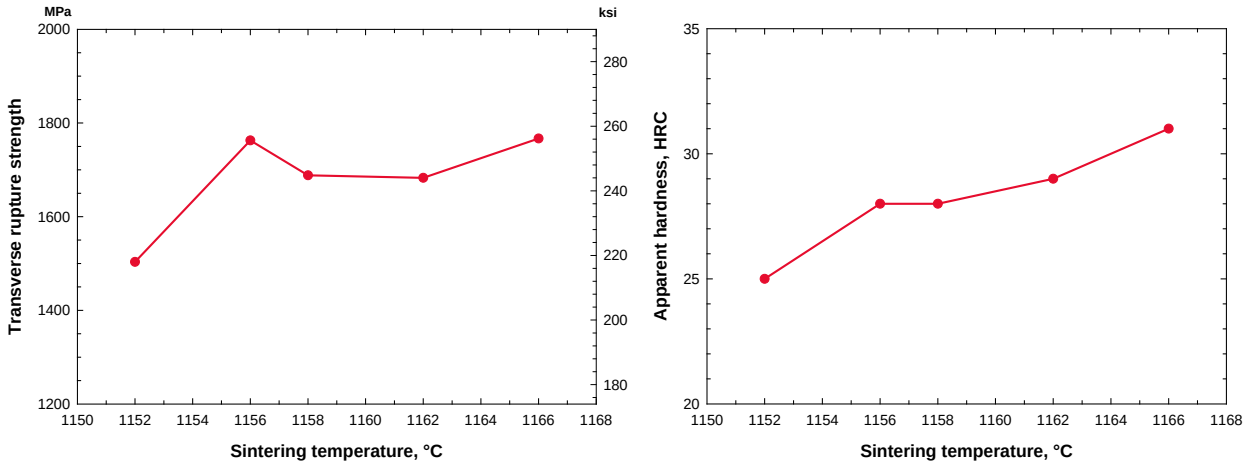

Figure 15. Evolution of transverse rupture strength and apparent hardness as a function of sintering temperature for specimens made of MIP.

Effect of green density on dimensional change after sintering

SLPS produces a large variation in final specimen dimensions. Therefore, the ability to hold tight tolerances with materials such as MIP, can prove to be a challenge. Compared to conventional PM steel, where the dimensional change usually varies about ±0.5% from die or green size, this new material will shrink by ~3.5% depending on the green density. Indeed, given that MIP parts typically sinter to a final density of 99% and above, the degree of shrinkage is governed primarily by green density. Figure 16 illustrates the impact of both the green and sintered density on dimensional change variation. The relationship between the dimensional change and the green and sintered densities, up to about 7.52 g/cm³ (99% relative density) where dimensional change levels off, is essentially linear. Indeed, dimensional change from die size can be mathematically expressed by the following equation:

Equation 1: DC (%) = -16.644 + 5.984 X (G.D., g/cm³) -3.535 X (S.D., g/cm³)

This equation illustrates that for sintered densities up to 7.52 g/cm³, a delta of 0.05 g/cm³ causes a variation of 0.18% of the final dimension for a given green density. On the other hand, for a sintered density of 7.52-7.57 g/cm³, a green density variation of 0.05 g/cm³ will induce a 0.30% change in the final dimension. This emphasizes the need to closely control the green density to minimize the variation in the final dimensions of MIP parts.

Axial fatigue and impact strength characterization

Previously, it was observed that for final sintered densities of 7.38 to 7.58 g/cm³, neither the density nor the shape of the graphite particles had a major effect on tensile properties. However, dynamic properties do not follow the same fracture mechanism. Indeed, the presence of residual porosity and variations in graphite cluster morphology are expected to affect fatigue resistance. To quantify these effects, rectangular bars were pressed to a range of densities and sintered at different temperatures. The sintered bars were machined into round specimens and axial fatigue tested at 100 Hz with a load ratio of R = -1. After testing, the density of the specimens was measured in the fracture area and the shape of the graphite particles evaluated by image analyses.

Figure 17 illustrates the variation of axial fatigue strength with density and the number of graphite flakes/mm² having a dimension larger than 100 µm. Fatigue strength is very sensitive to both the density and the shape of the graphite particles. Indeed, when the number of flakes > 100 µm is approximately 1/mm², the fatigue strength increases from 240 MPa (35 ksi) to 280 MPa (41 ksi) when the density increases from 7.40 g/cm³ (97.6% relative density) to 7.53 g/cm³ (99.3% relative density). These values are close to those achieved with Fe2Cu5C forged materials[21], (i.e. 294 MPa 43 ksi). However, the effect of sintered density becomes negligible as the number of large flakes increases above 4/mm². This clearly illustrates that in addition to the sintered density, the microstructure and more particularly the shape of the free graphite particles must be closely controlled to minimize its detrimental effect on fatigue strength.

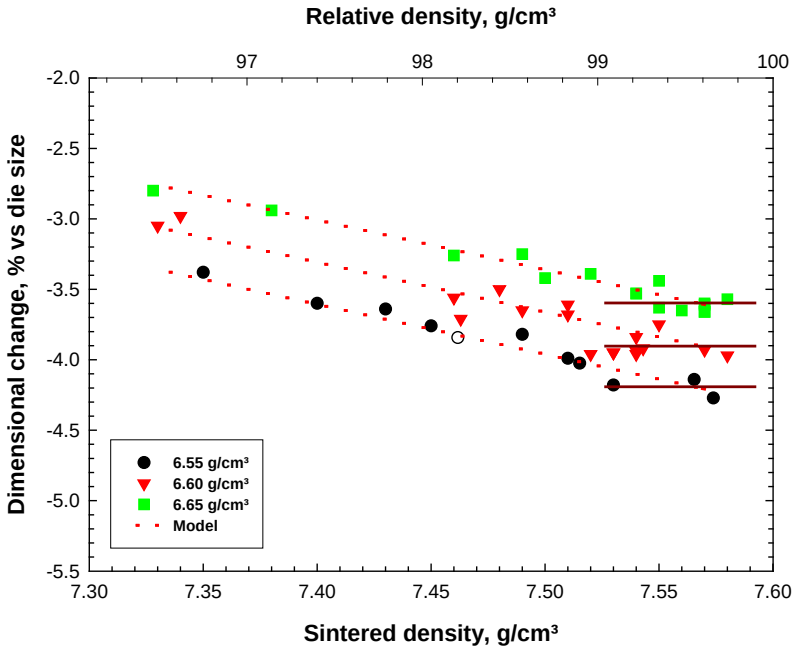

Figure 16. Variation of dimensional change with green and sintered density of specimens pressed with MIP (mix with 0.5% wax).

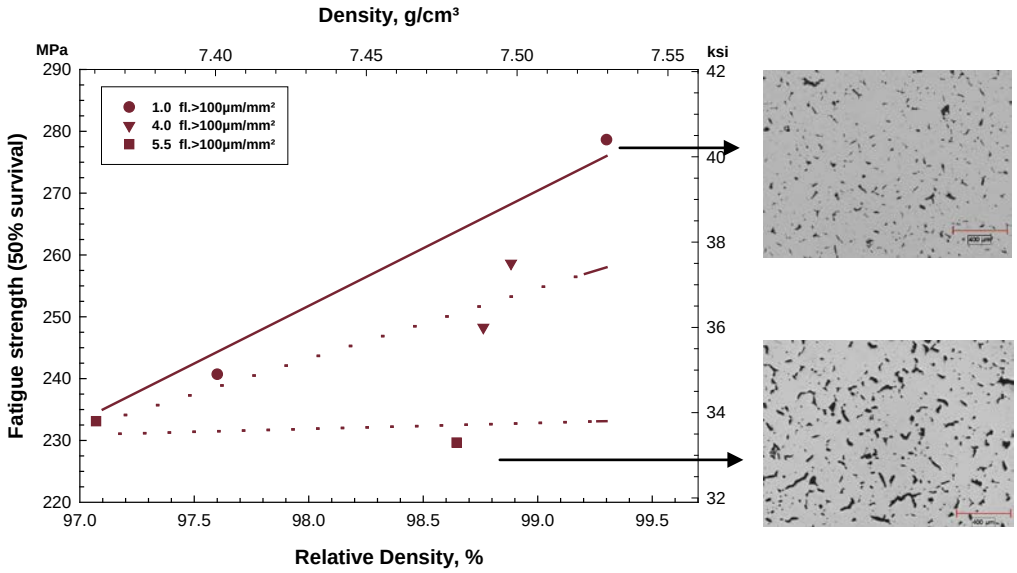

Figure 17. Effect of density and number of graphite flakes/mm² >100 µm on axial fatigue strength at R = -1 of specimens made with MIP.

Figure 18 compares the impact energy of MIP materials for two sintered densities and microstructures. The impact energy of this material is not as sensitive as fatigue resistance to density and microstructural variation. Indeed, impact energy values of about 32 J (24 ft-lb) are reached for densities of 7.52 g/cm³ and the effect of the number of large flakes is negligible.

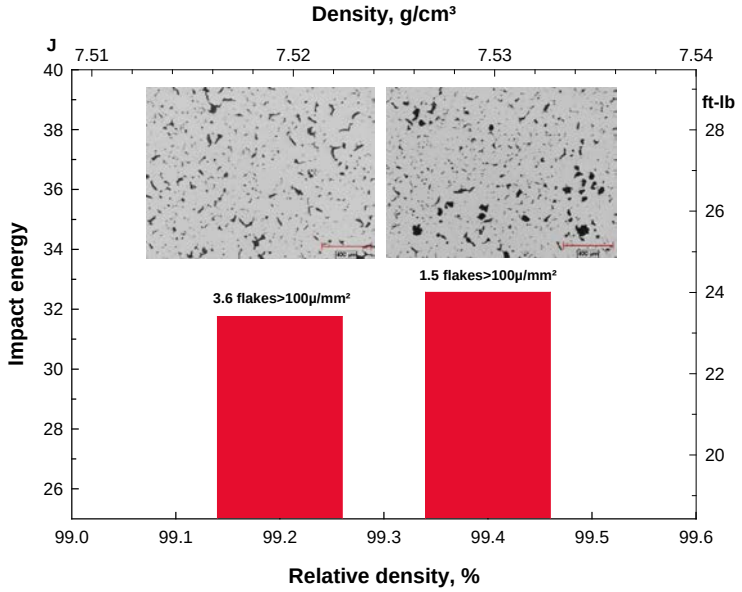

Figure 18. Impact energy of specimens made with MIP.

CONCLUSIONS

A new Fe-2C-1Si powder grade has been developed by a malleabilization treatment of a water atomized melt to achieve good compressibility. The resulting powder can be sintered to a relative density of 99%

(>7.50 g/cm³) through SLPS. The sintering temperature profile can be controlled to generate a fully pearlitic matrix structure with free graphite particles.

Tensile strength, yield strength and elongation were not significantly affected by the sintered density in a range of 97.1 to 99.9% (7.38-7.58 g/cm³) with values of 776 MPa (113 ksi), 523 MPa (76 ksi) and 2.2%, respectively. These properties are comparable to those of DI 100-70-3 and malleable cast iron class 80002.

Axial fatigue strength increases with sintered density and is affected by the shape of the free graphite flakes, which must be maintained below 4 flakes>100 µm/mm². A mean axial fatigue strength at R= -1 of 280 MPa (41 ksi) was reached at a density of 99.3% (7.53 g/cm³) with a proper microstructure.

An impact energy of 32 J (24 ft-lb) was measured at a sintered density of 99.3% and was not sensitive to the length of the graphite flakes.

REFERENCES

1. Poszmik, G, Luk, S.H.; "Binder treated Products for Higher Densities and Better Precision", Proceeding of the 2003 PM^{2}TEC Conference, MPIF, Princeton, 2003, part 3, pp33-44.
2. Chagnon F., St-Laurent, S.; "Optimizing Powder Mix Formulations and Processing Conditions for Warm Compaction", Proceeding of the 2000 Powder Metallurgy World Congress, Japan Society of Powder and Powder Metallurgy, Kyoto, 2000, part 1, pp543-546.
3. Lemieux, P., Azzi, L. Pelletier, S., Mongeon, P.E., St-Laurent, S.; "Pressing Challenging Parts on a Production Scale by Using Die Wall Lubrication Technology", Proceeding of the 2005 Advances in Powder Metallurgy & Particulates Materials Conference, MPIF, Princeton, 2005, part 3, pp. 71-83.
4. S. St-Laurent, Thomas, Y., Azzi, L; "High Performance Lubricants for Demanding PM Applications"; Proceeding of the 2006 Advances in Powder Metallurgy & particulate Materials Conference, MPIF, Princeton,. 2006, vol. 1, pp. 3-1 to 3-13.F. Chagnon; "Effect of powder characteristics, mix formulation and compacting parameters on green density of PM parts", Proceeding of the 2010 Advances in Powder Metallurgy & particulate Materials Conference, MPIF, Princeton,. 2010, vol. 1, pp. 3-34 to 3-44.
5. Hanejko, F.; "Single Press/Single Sinter Solutions to High Density"; Proceeding of the 2009 EURO PM, EPMA, Copenhagen 2009.
6. Donaldson, I.W.; "Utilizing an Advance Binder System for Achieving High Densities in Hybrid and Diffusion-Alloyed Materials", Proceeding of the 2005 Advances in Powder Metallurgy & particulate Materials Conference, MPIF, Princeton,. 2005, part 3, pp. 208-219.
7. Engtröm, U., Johansson, B., Knutsson, P., Vidarsson, H.; "Material Properties and Process Robustness Obtained with Warm Compaction of Improved DENSMIX™ Powders", Proceeding of the 2002 Advances in Powder Metallurgy & particulate Materials Conference, MPIF, Princeton,. 2002, part 4, pp. 118-129.
8. German, R.M.; "A Quantitative Theory for Supersolidus Liquid Phase Sintering", Powder Metallurgy, 1991, vol. 34, No. 2, pp 101-107.
9. German, R.M.; "Powder Metallurgy Science", Metal Powder Industries Federation, Princeton, 1994, p. 281.
10. www.calphad.com.
11. Kimura, T, Majima, A. and Kameoka, T.; "Supersolidus Hot Pressing of Ferrous P/M Alloys", The International Journal of Powder Metallurgy & Powder Technology, January 1976, vol. 12, no. 1, pp 19-23.

12. Shivanath, R., Kucharski, K and Jones, P.; “Press and Sinter Process for High Density Components”, US patent 6,346,213.
13. Young, E.; “High Density Supersolidus Liquid Phase Sintering of Steel Powders”, M. Sc. Thesis, The University of British Columbia, 2001.
14. Khraisat, W., Borgström, H., Nyborg, L. and Abu al Jadayil, W.; “Optimizing Grey Iron Powder Compacts”, Powder Metallurgy, 2009, vol. 52, no 4, pp 291-297.
15. Semel, F.J.; “Method of Preparing High Density Powder Metallurgy Parts by Iron based Infiltration”, US Patent Application US 2005/0142025.
16. Smith, W.F. “Structure and Properties of Engineering Alloys”, McGraw-Hill, New York, 1981, pp 315-361.
17. Metal Handbook, 9th edition, Volume 15; “Casting”, ASM International, Metals Park, 1988, pp 686-697.
18. www.foundryworld.com
19. Gagné, M., Filippelli, P. and Trudel, A.; “Iron-Graphite Composite Powders and Sintered Articles Produced Therefrom”, US Patent 6,358,298.
20. Ilia, E., O’Neill, M., Tutton, K., Lanni, G., Letourneau, S. and Haehnel, M.; “Benchmarking the Industry : Powder Forging Makes a Better Connecting Rod”; paper 2005-01-0713, Society of Automotive Engineers. Inc., 2005.